

Article

Not peer-reviewed version

High-Bandwidth Silicon Strip Waveguide-Based Optical Modulator in Series Push-Pull Configuration

[Ahmed Shariful Alam](#)^{*}, [Sherif Nasif](#), J. Stewart Aitchison

Posted Date: 4 April 2025

doi: 10.20944/preprints202504.0381.v1

Keywords: capacitive coupling; bandwidth enhancement; silicon modulators; series push-pull configuration




Preprints.org is a free multidisciplinary platform providing preprint service that is dedicated to making early versions of research outputs permanently available and citable. Preprints posted at Preprints.org appear in Web of Science, Crossref, Google Scholar, Scilit, Europe PMC.

Copyright: This open access article is published under a Creative Commons CC BY 4.0 license, which permit the free download, distribution, and reuse, provided that the author and preprint are cited in any reuse.

Article

High-Bandwidth Silicon Strip Waveguide-Based Optical Modulator in Series Push-Pull Configuration

Ahmed Shariful Alam ^{1,*} , Sherif Nasif ¹ and J. Stewart Aitchison ¹

Department of Electrical & Computer Engineering, University of Toronto, Toronto, ON M5S 1A4, Canada

* Correspondence: as.alam@mail.utoronto.ca

Abstract: Silicon modulators play a crucial role in optical communication systems. Over the past thirty years, there has been a notable enhancement in the bandwidth of silicon modulators; however, their operational speed remains constrained by the resistance-capacitance (RC) time constant. This study presents a silicon strip waveguide-based modulator configured in a series push-pull (SPP) arrangement, which effectively mitigates the limitations imposed by the RC time factor. The modulator exhibits a flat electro-optic (EO) response extending up to 68 GHz. Additionally, it achieves a phase shift of 0.022 radians for a C-band optical wave when subjected to a 15 GHz radio-frequency (RF) modulation signal with an amplitude of 2.45 V.

Keywords: capacitive coupling; bandwidth enhancement; silicon modulators; series push-pull configuration

1. Introduction

Integrated modulators are key components in modern optical communication systems, especially in short-reach optical communication systems [1–3]. Silicon-on-insulator (SOI) based integrated modulators are attractive for their CMOS (complementary metal-oxide semiconductor) compatibility, high bandwidth, and low insertion loss. Among the different types of silicon modulators, the depletion type silicon modulator is the most popular in the field of optical communications because of its high-speed operation. In most cases the depletion type silicon modulator consists of a rib waveguide with a lightly doped lateral PN diode in the core region and metal electrodes placed on the highly doped silicon slabs on either side of the waveguide core region. For high-speed operation such modulators are operated in the reverse bias regime [4]. The bandwidth of these modulators are limited to ~40 GHz because of the RC time constant which comes from the highly doped silicon slabs [5]. Although the bandwidth of silicon modulators has been enhanced using travelling wave electrodes (TWE) [6], segmented TWEs [7], and slow light effects [8], very few approaches have been made to get rid of the RC time limitation. In our previous reports, we have demonstrated a novel approach to enhance the bandwidth by coupling the electrical signal to the waveguide core capacitively. We also demonstrated a silicon strip waveguide-based silicon modulator or a capacitively coupled silicon (CC-Si) Mach-Zehnder interferometer (MZI) modulator in single drive configuration [9–11].

In this paper, we present a CC-Si MZI modulator configured in a series push-pull (SPP) arrangement, which was fabricated in a multi-project wafer (MPW) run at the Advanced Micro Foundry (AMF). The EO characterization of the modulator reveals the capability to generate sidebands reaching frequencies of up to 68 GHz around a continuous wave (CW) optical carrier in the C-band, with a flat EO response observed across this frequency range. Notably, for an RF modulation signal of 15 GHz, a linear correlation was established between the phase shift of the C-band optical carrier and the amplitude of the RF modulation signal. Specifically, the phase shift of the optical signal was observed to increase from 0.014 radians to 0.022 radians in a linear manner as the RF signal amplitude was elevated from 1.35 V to 2.45 V.

3. Experimental Demonstration

To demonstrate the EO response of the CC-Si MZI modulator in SPP configuration we built an experimental setup in Figure 1(f). A high-power RF signal generator which can generate sinusoidal signal up to 70 GHz with +25 dBm power was used. The RF signals are applied between the signal and ground terminal of the MZI. A 50 Ω termination load is used to terminate the other end of the RF transmission line of the modulator. A negative DC bias should be applied to the DC bias contact, however, the RF signal generator is very sensitive to the DC voltages and therefore, for the safety of the instrument we avoid applying any DC bias. We use a tunable laser source (TLS) to generate a +9 dBm CW optical carrier at 1550.31 nm wavelength which is near the quadrature point of the MZI. The optical carrier is coupled to the chip using a grating coupler after passing through a polarization controller (PC). The coupled optical carrier signal is split into two MZI arms using a 1×2 multimode interference (MMI) coupler. After phase modulation optical signals from both arms are combined using a 2×2 MMI coupler. These modulated optical signals are coupled out of the chip using two other grating couplers. One of the modulated signals is detected by a high-resolution optical spectrum analyzer (OSA). In this way, we can generate sidebands up to 68 GHz, which can be seen from Figure 2(a). The frequency dependent modulation indices, $m(f_m)$ is calculated from the carrier-sideband power ratio expressed by Eq. 1 [12].

$$R_{1,0} = \frac{J_1^2(m)}{1 + J_0^2(m) + 2J_0(m)\cos\phi} = \frac{I(\omega_0 + \omega_m)}{I(\omega_0)} \quad (1)$$

Here, ω_0 and $\omega_m (=2\pi f_m)$ are the optical carrier frequency and frequency of the modulation RF signals respectively. ϕ is the constant phase difference between two arms of the unbalanced MZI. J_0 and J_1 are the Bessel functions of first kind for orders 0 and 1 respectively. Carrier nulling is difficult to achieve in this case due to the distortions of the \cos^2 function of an unbalanced MZI CC-Si modulator and noise. To reduce the relevant uncertainties, the normalized transmission spectrum of the unbalanced MZI modulator is measured over a wider spectral range that includes the current operating optical carrier. In order to estimate the exact phase shift, ϕ , a fit of a model function of an unbalanced MZI modulator shown in Eq. 2 is performed with the experimental data.

$$T_{\text{UMZI}}(\omega) = A_0 + A_1 \cos^2 \left(\frac{1}{2} \left(B_0 + B_1(\omega - \omega_c) + B_2(\omega - \omega_c)^2 \right) \right) \quad (2)$$

In Eq. 2, $B_0 = \beta^{(0)} \Delta L$, $B_1 = \beta^{(1)} \Delta L$, and $B_2 = \frac{1}{2} \beta^{(2)} \Delta L$ where, ΔL is the path length difference between the two arms of the MZI, and $\beta^{(0)}$, $\beta^{(1)}$ and $\beta^{(2)}$ are the propagation constant, the first and the second order derivatives of the propagation constant respectively. ω_c is the center frequency of the frequency range of the unbalanced MZI spectrum. The fitting parameters A_0 , A_1 , B_0 , B_1 , and B_2 are determined using the least-square fit method. The phase shift, ϕ of an unbalanced CC-Si MZI modulator can be calculated from Eq. 3.

$$\phi = \frac{1}{2} \left(B_0 + B_1(\omega - \omega_c) + B_2(\omega - \omega_c)^2 \right) \quad (3)$$

After eliminating the effect of the grating couplers, the measured transmission spectrum is shown by the blue circles in Figure 2(b). The fit to the measured data using Eq. 2 is shown by the red line in Figure 2(b) and the operating optical carrier is pointed out with a green circle in Figure 2(b). The phase shift value, ϕ , and the carrier to sideband ratio, $R_{1,0}$ are used to calculate the $m(f_m)$ using Eq. 1, the blue line of Figure 2(c). The signal generator can generate a power of +25 dBm for all frequencies. However, the losses of the RF probes and the RF cable are frequency dependent. Hence, the RF power which is actually applied at the modulator terminal is microwave frequency dependent. We measure the RF power for different frequencies using an RF power meter. The associated frequency dependent peak voltages, $V(f_m)$ based on these RF power measurements are plotted in the red line of Figure 2(c). It is observed that the curve of $m(f_m)$ follow the curve of $V(f_m)$. Later, the $m(f_m)$ curve is normalized

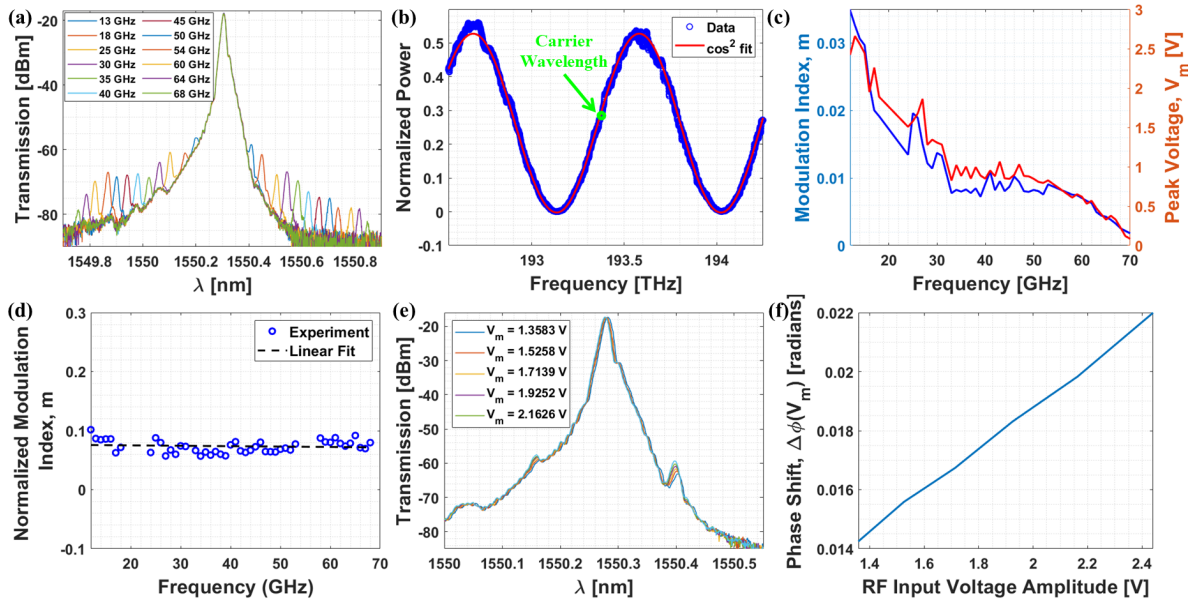


Figure 2. (a) Transmission spectra of the modulated optical signal for RF signal of different frequencies. (b) Measured intensity spectra of an unbalanced MZI CC-Si modulator (blue circles) in SPP configuration and associated fit (red line) according to Eq. 2. The carrier wavelength is pointed out with a green circle. (c) Frequency dependent $m(f_m)$ (blue line) and associated $V(f_m)$ (red line). (d) Normalized $m(f_m)$ and associated linear fit. (e) Transmission spectra of modulated optical signal for different RF power at 15 GHz. (f) Voltage dependent phase shift, $\phi(V_m)$ at 15 GHz.

with respect to a frequency independent +2 dBm RF power which is plotted in Figure 2(d). A linear fit of the normalized $m(f_m)$ is also shown in Figure 2(d) which shows that the CC-Si MZI modulator has a very flat frequency response.

Followed by the EO measurement, we measure transmission spectra of different modulated optical signals for 15 GHz RF sinusoidal signals with different powers i.e., different peak voltage, V_m . The measured transmission spectra are shown in Figure 2(e). Before applying the 15 GHz RF signals, we measure the powers of different RF signals using an RF power meter. Thus, we determine the phase shift, $\phi(V_m)$ for 15 GHz RF-signal which is voltage dependent. Figure 2(f) shows the phase shifts for different RF powers i.e., different V_m of 15 GHz signals. We observe a linear relationship between V_m and $\phi(V_m)$. ϕ increase from 0.014 radians to 0.022 radians almost linearly as the amplitude of the 15 GHz RF signal was raised from 1.35 V to 2.45 V. These devices are expected to have comparatively lower phase shifts, since we use silicon dioxide cladding with low dielectric constant that reduces the electrical field confinement within the waveguide region [9].

4. Conclusions

To summarize, we have demonstrated a CC-Si modulator which can enhance the bandwidth of silicon devices by eliminating the RC time limitation. Lumerical Device simulations were performed to show the working principle of the CC-Si modulator. We performed the EO measurement of a CC-Si MZI modulator in SPP configuration and observe a flat EO frequency response up to 68 GHz which proves the broadband nature of this device. 15 GHz RF modulation signals with different amplitudes were used to calculate the voltage dependent phase shift, $\phi(V_m)$. We observed almost linear relationship between the phase shift of a C-band optical carrier and the amplitude of the RF modulation signal. The phase shift of the optical signal increased from 0.014 radians to 0.022 radians almost linearly while the RF signal amplitude was elevated from 1.35 V to 2.45 V.

The EO response of the CC-Si modulator clearly shows that it will be flat beyond 68 GHz. We are currently limited by the RF power and the maximum frequency provided by the signal generator. The $V_\pi L$ of this modulator is high due to the low dielectric constant silicon dioxide ($\epsilon_{\text{SiO}_2} = 3.9$) cladding [13]

around a comparatively higher dielectric constant silicon ($\epsilon_{\text{Si}} = 11.9$) waveguide [14] which results in more electrical field drop outside of the waveguide core. This limitation can be improved by replacing the silicon dioxide cladding with a very high dielectric constant material like barium titanate which has been found effective in different platforms like silicon-organic hybrid (SOH) platform [15–18] and lithium niobate-on insulator (LNOI) platform [19–21]. However, deposition of a high dielectric constant material is not a standard for existing silicon photonic foundries. But we are currently investigating this approach by doing back-end-of-line (BEOL) post-fabrication processes. Moreover, due to the resolution of the OSA we chose a sideband at comparatively higher frequency (15 GHz) of RF signal where different other factors such as impedance mismatch, microwave propagation loss, velocity mismatch between the optical and the RF mode play a significant role. Thus, the voltage dependent phase shift, $\phi(V_m)$ in such high frequency will be much lower compared to the phase shift values measured at kHz range frequencies. Also, for the safety of the signal generator no DC bias is applied which leads to higher chirping by generating positive Δn_{eff} in both MZI arms. As a result, the differential phase shift between two arms is smaller than the phase shift with a negative DC bias. Thus, the absence of negative DC bias leads to lower phase shifts. Additionally, without any DC bias for half-cycle of an RF modulation sinusoidal signal the PN diode will be in forward bias which can potentially limit the bandwidth of the device. Nevertheless, with progress in characterization and fabrication techniques we believe that these challenges can be solved which will allow high-performance devices.

Funding: This work is supported by the Natural Sciences and Engineering Research Council of Canada (NSERC) discovery grant (RGPIN-2022-04871), and by CMC Microsystems.

Data Availability Statement: The data sets generated and/or analyzed during the current study are available from the corresponding authors on reasonable request.

Acknowledgments: We express our gratitude to Prof. Joyce Poon for her assistance in characterizing the device. We also thank Prof. George Eleftheriades & Alex MacKay for use of the high-power signal generator and the RF power meter, and Prof. Li Qian & Alexander Greenwood for access to the high-resolution optical spectrum analyzer.

Conflicts of Interest: The authors declare no conflict of interest.

Abbreviations

The following abbreviations are used in this manuscript:

RC	Resistance-capacitance
SPP	Series push-pull
RF	Radio-frequency
CMOS	Complementary metal-oxide semiconductor
TWE	Traveling wave electrode
CC-Si	Capacitively coupled silicon
MZI	Mach-Zehnder interferometer
MPW	Multi-project wafer
AMF	Advanced Micro Foundry
EO	Electro-optic
CW	Continuous wave
PN	P-type/N-Type
DC	Direct current
TLS	Tunable laser source
PC	Polarization controller
MMI	Multimode interference
OSA	Optical spectrum analyzer
LNOI	Lithium niobate on insulator
BEOL	Back-end-of-line

References

1. Dong, P.; Lee, J.; Chen, Y.K.; Buhl, L.L.; Chandrasekhar, S.; Sinsky, J.H.; Kim, K. Four-channel 100-Gb/s per channel discrete multi-tone modulation using silicon photonic integrated circuits. In Proceedings of the 2015 Optical Fiber Communications Conference and Exhibition (OFC), 2015, pp. 1–3. <https://doi.org/10.1364/OFC.2015.Th5B.4>.
2. Xie, C.; Magill, P.; Li, D.; Zhang, Y.; Zheng, L.; Wang, A.; Bao, Y.; Sui, C.; Streshinsky, M.; Mu, J.; et al. Real-Time Demonstration of Silicon-Photonics-Based QSFP-DD 400GBASE-DR4 Transceivers for Datacenter Applications. In Proceedings of the 2020 Optical Fiber Communications Conference and Exhibition (OFC), 2020, pp. 1–3. <https://doi.org/10.1364/OFC.2020.T3H.5>.
3. Yu, H.; Patel, D.; Liu, W.; Malinge, Y.; Doussiere, P.; Lin, W.; Gupta, S.; Narayanan, K.; Hoshino, I.; Bresnahan, M.; et al. 800 Gbps Fully Integrated Silicon Photonics Transmitter for Data Center Applications. In Proceedings of the 2022 Optical Fiber Communications Conference and Exhibition (OFC), 2022, pp. 1–3. <https://doi.org/10.1364/OFC.2022.M2D.7>.
4. Liao, L.; Liu, A.; Rubin, D.; Basak, J.; Chetrit, Y.; Nguyen, H.; Cohen, R.; Izhaky, N.; Paniccia, M. 40 Gbit/s silicon optical modulator for high-speed applications. *Electronics Letters* **2007**, *43*, 1196–1197. <https://doi.org/10.1049/el:20072253>.
5. Watts, M.R.; Zortman, W.A.; Trotter, D.C.; Young, R.W.; Lentine, A.L. Low-Voltage, Compact, Depletion-Mode, Silicon Mach-Zehnder Modulator. *IEEE Journal of Selected Topics in Quantum Electronics* **2010**, *16*, 159–164. <https://doi.org/10.1109/JSTQE.2009.2035059>.
6. Zhang, H.; Li, M.; Zhang, Y.; Zhang, D.; Liao, Q.; He, J.; Hu, S.; Zhang, B.; Wang, L.; Xiao, X.; et al. 800 Gbit/s transmission over 1 km single-mode fiber using a four-channel silicon photonic transmitter. *Photon. Res.* **2020**, *8*, 1776–1782. <https://doi.org/10.1364/PRJ.396815>.
7. Mohammadi, A.; Zheng, Z.; Lin, J.; Rad, M.M.; Zhang, X.; Rusch, L.A.; Shi, W. Segmented Silicon Photonic Modulator with a 67-GHz Bandwidth for High-Speed Signaling. In Proceedings of the Optical Fiber Communication Conference (OFC) 2022. Optica Publishing Group, 2022, p. Th3C.1. <https://doi.org/10.1364/OFC.2022.Th3C.1>.
8. Han, C.; Zheng, Z.; Shu, H.; Jin, M.; Qin, J.; Chen, R.; Tao, Y.; Shen, B.; Bai, B.; Yang, F.; et al. Slow-light silicon modulator with 110-GHz bandwidth. *Science Advances* **2023**, *9*, eadi5339. <https://doi.org/10.1126/sciadv.adi5339>.
9. Alam, A.S.; Sun, H.; Masnad, M.; Alamgir, I.; na, J.A.; Aitchison, J.S. Carrier Dispersion Modulation in a Silicon Strip Waveguide. In Proceedings of the CLEO 2024. Optica Publishing Group, 2024, p. JTh2A.195. https://doi.org/10.1364/CLEO_AT.2024.JTh2A.195.
10. Alam, A.S.; Sun, H.; Masnad, M.M.; Alamgir, I.; Azaña, J.; Aitchison, J.S. Bandwidth Estimation of a Silicon Strip Waveguide Based Optical Modulator. In Proceedings of the Frontiers in Optics + Laser Science 2024 (FiO, LS). Optica Publishing Group, 2024, p. JW4A.50. <https://doi.org/10.1364/FIO.2024.JW4A.50>.
11. Alam, A.S.; Aitchison, J.S. Capacitively Coupled Silicon Modulator Fabricated on the Standard Silicon-on-Insulator Platform. *IEEE Photonics Journal* **2025**.
12. Shi, Y.; Yan, L.; Willner, A. High-speed electrooptic modulator characterization using optical spectrum analysis. *Journal of Lightwave Technology* **2003**, *21*, 2358–2367. <https://doi.org/10.1109/JLT.2003.818162>.
13. Reynard, J.; Verove, C.; Sabouret, E.; Motte, P.; Descouts, B.; Chaton, C.; Michailos, J.; Barla, K. Integration of fluorine-doped silicon oxide in copper pilot line for 0.12- μm technology. *Microelectronic Engineering* **2002**, *60*, 113–118. Materials for Advanced Metallization, [https://doi.org/10.1016/S0167-9317\(01\)00586-X](https://doi.org/10.1016/S0167-9317(01)00586-X).
14. Alfaraj, N.; Lin, C.C.C.; Nasif, S.; Rajput, S.; Helmy, A.S. Facile integration of electro-optic SiO₂/ITO heterointerfaces in MIS structures for CMOS-compatible plasmonic waveguide modulation. *Light: Advanced Manufacturing* **2023**, *4*, 420. <https://doi.org/10.37188/lam.2023.038>.
15. Alam, A.S. Design, Fabrication and Characterization of Capacitively Coupled Silicon-Organic Hybrid Modulators. Master's thesis, Karlsruhe Institute of Technology (KIT), 2017. <https://doi.org/10.5445/IR/1000160228>.
16. Ummethala, S.; Kemal, J.N.; Lauermann, M.; Alam, A.S.; Zwickel, H.; Harter, T.; Kutuvantavida, Y.; Hahn, L.; Nandam, S.H.; Elder, D.L.; et al. Capacitively Coupled Silicon-Organic Hybrid Modulator for 200 Gbit/s PAM-4 Signaling. In Proceedings of the Conference on Lasers and Electro-Optics. Optica Publishing Group, 2019, p. JTh5B.2. https://doi.org/10.1364/CLEO_AT.2019.JTh5B.2.
17. Ummethala, S.; Kemal, J.N.; Alam, A.S.; Lauermann, M.; Kuzmin, A.; Kutuvantavida, Y.; Nandam, S.H.; Hahn, L.; Elder, D.L.; Dalton, L.R.; et al. Hybrid electro-optic modulator combining silicon photonic slot

- waveguides with high-k radio-frequency slotlines. *Optica* **2021**, *8*, 511–519. <https://doi.org/10.1364/OPTICA.411161>.
18. Ummethala, S. Plasmonic-Organic and Silicon-Organic Hybrid Modulators for High-Speed Signal Processing. PhD thesis, Karlsruhe Institute of Technology (KIT), 2021. 43.32.03; LK 01, <https://doi.org/10.5445/IR/1000136059>.
 19. Alam, A.S.; Aitchison, J.S. Low Half-Wave-Voltage Lithium Niobate Modulator Using High-K Dielectric Material Cladding. In Proceedings of the Optica Advanced Photonics Congress 2022. Optica Publishing Group, 2022, p. JTU2A.9. <https://doi.org/10.1364/BGPPM.2022.JTu2A.9>.
 20. Alam, A.S.; Aitchison, J.S. Optimization of a Broadband Lithium Niobate-Barium Titanate Hybrid Modulator With Low Half-Wave-Voltage-Length Product. *IEEE Photonics Journal* **2023**, *15*, 1–7. <https://doi.org/10.1109/JPHOT.2023.3329781>.
 21. Chen, N.; Lou, K.; Yu, Y.; He, X.; Chu, T. High-Efficiency Electro-Optic Modulator on Thin-Film Lithium Niobate with High-Permittivity Cladding. *Laser & Photonics Reviews* **2023**, *17*, 2200927. <https://doi.org/10.1002/lpor.202200927>.

Disclaimer/Publisher's Note: The statements, opinions and data contained in all publications are solely those of the individual author(s) and contributor(s) and not of MDPI and/or the editor(s). MDPI and/or the editor(s) disclaim responsibility for any injury to people or property resulting from any ideas, methods, instructions or products referred to in the content.